Unprecedented spike flexibility revealed by BSL3 Cryo-ET of active SARS-CoV-2 virions

Hideo Fukuhara[1,2,3,†], Hisham M. Dokainish[2,†,*], Shunsuke Kita[2], Koshiro Tabata[4,5], Akira Takasu[6], Juha T. Huiskonen[7], Yuki Anraku[2], Toshiya Senda[6,8,9], David I. Stuart[10], Michihito Sasaki[4], Yasuko Orba[4], Yasuhiko Suzuki[5,11,*], Hirofumi Sawa[4,5,12,13,*] & Katsumi Maenaka[1,2,3,5,12,14,*].

Affiliations:

[1] Division of Pathogen Structure, International Institute for Zoonosis Control, Hokkaido University, Kita-20, Nishi-10, Kita-ku, Sapporo 001-0020, Japan.

[2] Laboratory of Biomolecular Science and Center for Research and Education on Drug Discovery, Faculty of Pharmaceutical Sciences, Hokkaido University, Kita-12, Nishi-6, Kita-ku, Sapporo 060-0812, Japan.

[3] Global Station for Biosurfaces and Drug Discovery, Hokkaido University, Kita-12, Nishi-6, Kita-ku, Sapporo 060-0812, Japan

[4] Division of Molecular Pathobiology, International Institute for Zoonosis Control, Hokkaido University, Kita-20, Nishi-10, Kita-ku, Sapporo 001-0020, Japan

[5] Institute for Vaccine Research and Development (HU-IVReD), Hokkaido University, Kita-21, Nishi-11, Kita-ku, Sapporo 001-0020, Japan

[6] Structural Biology Research Center, Institute of Materials Structure Science, High Energy Accelerator Research Organization (KEK), Tokyo 135-0063, Japan

[7] Institute of Biotechnology, Helsinki Institute of Life Science HiLIFE, University of Helsinki, P.O. Box 56, 00014 Helsinki, Finland.

[8] Department of Accelerator Science, School of High Energy Accelerator Science, SOKENDAI (the Graduate University for Advanced Studies), 1-1 Oho, Tsukuba, Ibaraki 305-0801, Japan

[9] Faculty of Pure and Applied Sciences, University of Tsukuba, 1-1-1 Tennodai, Tsukuba, Ibaraki 305-8572, Japan

[10] Division of Structural Biology, University of Oxford, The Wellcome Centre for Human Genetics, Headington, Oxford OX3 7BN, UK; Chinese Academy of Medical Sciences Oxford Institute, University of Oxford, Oxford OX3 7FZ, UK; Diamond Light Source Ltd, Harwell Science & Innovation Campus, Didcot OX11 0DE, UK; Nuffield Department of Medicine, Wellcome Centre for Human Genetics, University of Oxford, Oxford OX3 7BN, UK.

[11] Division of Bioresources, International Institute for Zoonosis Control, Hokkaido University, Kita-20, Nishi-10, Kita-ku, Sapporo 001-0020, Japan

[12] One Health Research Center, Hokkaido University, Kita-19, Nishi-9, Kita-ku, Sapporo 001-0020, Japan

[13] Global Virus Network, Baltimore, Maryland, USA

[14] Faculty of Pharmaceutical Sciences, Kyushu University, Fukuoka, 812-8582, Japan.

*Corresponding authors. Email: suzuki@czc.hokudai.ac.jp (Y.S.); hisham.dokainish@pharm.hokudai.ac.jp (H.M.D.); h-sawa@ivred.hokudai.ac.jp (H.S.); maenaka@pharm.hokudai.ac.jp (K.M.; Lead contact)

† These authors contributed equally to this work

Abstract:

Understanding the molecular properties of SARS-CoV-2 is crucial to tackle future outbreaks. Current knowledge of the trimeric spike protein relies on truncated recombinant proteins and inactivated full-length forms, which may suffer from overstabilization. Here, we apply cryo-electron tomography (cryo-ET) at a Biosafety level 3 facility to study the virus structure in its native, active state. The virus particles show variable shapes with diffusible spikes, with the majority in typical prefusion conformations. Notably, we also identified unprecedented, atypical open-trimer prefusion states, revealing hidden flexibility. The sub-tomogram averaged structure suggests a loosely packed trimer. The observed dynamics uncover conserved cryptic regions that can be targeted for broadly effective vaccines. Structural analysis of active viruses will have implications on understanding overlooked fusion mechanism and vaccine, antibody/drug design. (124 words)

One-Sentence Summary: The BSL3 cryo-electron microscopy uncovered significant flexibility of the spike protein on active viruses, which will facilitate the design of broadly effective vaccines and drugs.

Main Text:

Severe acute respiratory syndrome coronavirus 2 (SARS-CoV-2) continues to impact global health(1). The ongoing emergence of new variants hinders the efficacy of developed vaccines and therapeutic antibodies(2, 3). The spike protein decorates the virus surface and plays central roles in the viral entry and immune shielding mechanisms(4, 5). The spike protein is a trimeric glycoprotein, wherein each protomer is formed of two subunits (S1 and S2) with a transmembrane region(6). Numerous studies elucidated spike protein structures and dynamics, paving the way for mRNA vaccine developments(6-10). Specifically, cryogenic electron microscopy (cryo-EM) has been used to determine structures of the recombinant spike protein in wild-type and emerging variants(3, 6-12). Moreover, cryogenic electron tomography (cryo-ET) has enabled the study of full-length spikes in the inactivated viruses, unraveling the flexibility of its stalk region and the protein distribution on the virus surface(7, 13-18). Structural studies provided fundamental information on the virus molecular structure, architecture, interactions, and dynamics(4).

Despite the enormous amount of structural information available on SARS-CoV-2 virus and its spike protein, our understanding of the virus in its active form is still lacking(19). In fact, the majority of cryo-EM studies are performed using a truncated ectodomain of the spike protein, which includes several mutations (e.g. 2P and 6P proline mutations) designed to stabilize the prefusion state(20, 21). Accordingly, several approved vaccines include similar proline mutations, for improving production and stabilization(22). Indeed, the proline mutations may induce local rigidity altering the nearby secondary structure(23). Likewise, to reduce biological hazards, chemical fixation is usually applied in cryo-ET experiments(15, 19). Chemicals such as paraformaldehyde (PFA) are known to react with amino residues and may cause morphological changes that alter protein structures(19, 24). In addition, electron (E)-beam inactivation was recently shown to be damaging to spike protein structures(15). According to previous structural studies, the spike protein has a reasonably stable prefusion state with a number of conformational states that are governed by the motion of its S1 receptor binding domains (RBDs) from Down to Up states(6). In contrast, Hydrogen Deuterium Exchange Mass Spectrometry (HDX-MS) study showed that the prefusion state of the spike protein is quite dynamic, highlighting the existence of a form of the prefusion state in which parts of S2 are exposed(23). Furthermore, the binding of some antibodies to the S2 subunit in the prefusion state suggests the formation of an unknown open trimer structure(25). Collectively, previous studies showed structural flexibility at several levels using artificially stabilized proteins and inactivated viruses. However, true images of spike proteins are still missing.

Understanding the differences between the current structural knowledge of SARS-CoV-2 that may suffer from overstabilization, and the active form is crucial for future vaccine and antibody/drug development. Certainly, elucidating the dynamics of spike proteins in its native form would shape the approach to targeting future variants. To address this point, we set up the high-end cryo-electron microscope at a Biosafety level 3 (BSL3) area to employ cryo-ET and single-particle tomography (SPT)(26) to unravel the structure of the spike protein using active viruses. In this experiment, neither chemical fixation nor ultracentrifugation were applied, to avoid spike structure alteration or detachment. To the best of our knowledge, this is the first structural study of SARS-CoV-2 in its active form.

Results

BSL3 High-end Cryo-electron Microscope.

We set up the latest generation of cryo-electron microscope (300 kV), Krios G4 (Thermo Fisher Scientific) with a Falcon 4 direct electron detector and a Selectris energy filter in the management area for BSL3 pathogens in the International Institute for Zoonosis Control, Hokkaido University (Fig. S1). The detail of BSL3 cryo-EM system and procedure for handling the grid preparation and data collection will be published elsewhere, but briefly, virus vitrification using EM GP2 (Leica) and autogrid assembly were performed in the safety cabinet. The autogrid was transferred to Krios G4 and cryo-ET data were collected (Fig. S1). The active SARS-CoV-2 of the ancestral strain WK-521 in cell culture was directly frozen and observed. Thus, the virus preparation did not include any ultracentrifugation or chemical fixation to avoid any kind of artifacts as much as possible.

The Pleomorphic Virus Particles Morphology.

Early cryo-ET study of the inactivated SARS-CoV-2 demonstrated the formation of an ellipsoidal or a spherical-shaped viral envelope, with an average of 96.6 nm for its longest axis(16). In contrast, a more recent cryo-ET study suggested the formation of a dominant flat cylindrical shape, in ancestral, alpha, beta and delta variants, with an average diameter of 102 nm(14). Notably, a later cryo-ET study of the delta variant has shown the formation of fused virus particles, where one envelope encloses two sets of RNPs(15). In summary, previous cryo-ET studies suggested some level of pleomorphism.

In this study, 42 tomograms of the active ancestral virus were recorded and reconstructed, including 46 virus particles (e.g. Movie S1). A tilt angular step of 1°, covering a range from −60° to +60° was used, resulting in 121 tilt images per tomogram. Fig. 1 shows a variety of envelope shapes, including dominant spherical (L1: 99 ± 13.6 nm, L2: 94 ± 13.6 nm) and ellipsoidal shapes (L1: 117 ± 19.7 nm, L2: 94 ± 15.9 nm), as well as oval (L1: 99 ± 21.5 nm, L2: 87 ± 10.6 nm), cylindrical (L1: 93 ± 7.9 nm, L2: 57 ± 10.1 nm) and bean-like (L1: 100 ± 12.7 nm, L2: 65 ± 10.9 nm) envelops (summarized in Table S1). The measured diameters of the two longest axes (L1 and L2) indicate a large variation in the virus size, wherein the maximum axis (L1) can vary from 72 to 150 nm (Movie S2). Remarkably, very large virus particles with L1:150, L2:125 (Fig. 1c right) and L1:139, L2:102 nm (Fig. 1c left) were observed. Such large particles may indicate the fusion of two virus particles in ancestral strain, as recently observed in delta variant(15). Fig. S2a and Movie S3 also show the observation of two virus particles apparently undergoing a fusion process. In addition, Fig. S2b suggests that there is no correlation between the observed morphology and ice thickness. It also shows that the third axis is correlated with the particle size. Collectively, unlike previous results from inactivated viruses that exhibit a dominant morphology, our results suggest a high level of flexibility, adaptability, and pleomorphism on virus shape in response to surrounding environments.

Spike Distribution and Arrangements.

In the current dataset, one-third of the particles (14 out of 46) were observed on the carbon film. These particles tend to include a higher density of spike proteins, in comparison to the ones in the grid holes. On the carbon, spike proteins are pushed to the edge of the flattened particle, reflecting high diffusibility within the native viral lipid membrane (Fig. 1d). Such high

diffusibility may allow the virus to relocate more spikes at the interface upon encountering natural host receptor, Angiotensin-converting enzyme 2 (ACE2). On the other hand, within grid holes, spike proteins are more dispersed on the surface, where fewer spikes can be identified in most cross sections. Fig. 2a shows that spike proteins can exist as a dimer of trimers or even a trimer of trimers (Movie S1 right), and similar complexes were previously observed in full-length spike proteins from the Novavax vaccine(27). Fig. S3a indicates the formation of two spike trimers with shared transmembrane regions, as reported previously(16). Such arrangements raise a question regarding the possibility of protomer swapping between trimeric spike structures. Both 247 prefusion and 44 postfusion conformations were observed across active virus particles. Specifically, the postfusion state was found to occur in clusters (Fig. 2b). The formation of postfusion clusters may facilitate membrane fusion by attaching several fusion peptides at the same time.

Atypical Spike Conformations Indicate an Open Trimer.

Fig. 2c and d show all typical forms of the spike protein observed in our dataset. This includes the prefusion Down, 1Up, 2Up and 3Up states, reflecting the inherent dynamical nature of the spike protein, in the absence of ACE2 or neutralizing antibody (nAb). Notably, besides typical conformations, atypical forms of the spike protein were also observed. Among these, spike protomers may undergo large conformational changes, forming novel open trimer states. Simple fitting to a detached density indicates that the observed motion involves the S1 subunit of single spike protomer. Accordingly, a range of open trimer structures can be seen (Fig. 2d, and 2e), exposing the S2 subunit. Furthermore, more open and distinct types of trimer structures exist (Fig. 2f and Fig. S3b). It is important to mention that, while the majority of spike protein conformations in our dataset were typical prefusion states, open trimer conformations occur in some portion (10~20 %) of observed prefusion states. These results suggest a hidden motion of the spike structure, in which spike protomers are more flexible and can undergo conformational opening (Fig. 2f). Consistently, previous HDX-MS studies using the recombinant ectodomain of the spike protein with a prefusion stabilization (2P mutations) suggested the minor presence of an alternative conformation, in which S2 residues are solvent exposed, which can be targeted by nAbs, such as 3A3 and RAY53(22, 23, 25). Therefore, in active viruses, the typical closed/packed prefusion conformation is dominant but the spike protein itself has ability to spontaneously transit to an open-trimer conformation.

Spike Average Conformation Suggests a Loosely Packed Structure.

To gain further insights into the mechanism of the open-trimer formation, we performed single particle tomography (SPT) analysis of the prefusion packed conformation. 237 prefusion spike particles were manually picked (excluding open trimer and postfusion states). Around 28,000 tilt images (121 tilt per particle) were used for the 3D re-construction, with a voxel size of 1.884 Å. To avoid any bias, no previously published maps of the spike protein were used in the alignment and refinement processes. Fig. 3a and Movie S4 show the sub-tomogram averaged map of the C3 symmetric spike protein, which was obtained with a global resolution of 14 Å (Fig. S4). In addition, a C1 symmetry map was also obtained at a slightly lower global resolution of 17.0 Å, and this was essentially similar to the C3 symmetric structure but with less density in one protomer (Fig. 3b). The general features of the maps obtained are similar to those of previous cryo-EM studies. A 2.6 Å resolution structure of the ancestral spike protein (PDB 6ZGE)(10) fits

adequately in the obtained low-resolution map (Fig. 3a bottom). However, a better fit was obtained using the asymmetrically refined structure (PDB 7M0J) of the engineered spike (u1S2q) with quadruple mutations (A570L, T572I, F855Y, N856I) (28, 29) (Fig. 3a top). Which was previously shown to exhibit intrinsic mobility, evidenced by high propensity of forming 1Up and 2Up conformations and sustained binding to the CR3022 antibody(29). In detail, the SPT map shows missing density at the S2 middle helices interface (Fig. 3a top center). The helices were elongated and contributed to forming tightly packed S2 in many reported cryo-EM structures, however, there exists some variation of S2 middle helices interface in cryo-EM structures. Our cryo-ET map fits better to the 7MOJ structure harboring slightly bent helices (Fig. 3a top center). Notably, the S2 subunit shows multiple regions with charged residues (Fig. S5) at the trimer interface and, in the 7MOJ structure, the S2 subunit makes hydrophobic interactions at the interface to avoid charge repulsion. In addition, Fig. 3a bottom center highlights the fitting of 6ZGE and 7M0J to the proximal part of the stem helices, wherein the 7M0J structure shows an upward shift that again better fit the averaged map. Previous principal component (PC) analysis of 165 protomers from 52 spike Down PDB structures, shows a similar behavior where PC1 and PC2 modes both show up and down motion in S2 with respect to S1, indicating structural variation within the available PDB structures(30). Therefore, these structural features allow for more flexible movement of the protomers and the formation of the above-mentioned open trimer structure as well as the transition to postfusion (Fig. 4). Notably, a recent sub-tomogram averaged map of Env protein (9.1 Å resolution) in intact HIV particles, has also suggested structural differences in middle helix region that suggest flexibility at the helical bundle core(13).

Discussion

Mutations of the spike protein are a major underlying cause for immune escape and reduction of vaccine efficiency. The development of broadly neutralizing antibodies (bnAbs) is important for preparedness for future pandemics. The recent review of Zhou et al. summarized three major non-RBD sites targeted for bnAbs, (1) fusion peptide, (2) SD1 (the S1 subdomain 1) and (3) the C-terminal stem helix(31). Our cryo-ET map shows that the spike protein is flexible enough for these sites to be to some extent exposed in open-trimer structures, possibly generating bnAbs that exhibit neutralizing activity but with less potency. Either cocktails or bispecific forms of bnAbs, which can recognize different epitopes of single spike protein spontaneously, may improve the activity and tolerate mutations(31).

The development of long-term and broadly effective vaccines also requires new strategies to target highly conserved epitope regions(32, 33). Unlike RBD which is a hot spot for mutations, the S2 subunit shows higher conservation, wherein few mutations have emerged since the start of the pandemic. In fact, the fusion peptide (FP) and heptad repeat regions (HR1 and HR2) of the S2 subunit are more conserved within all coronaviruses including SARS-CoV-1 and Middle East respiratory syndrome coronavirus (MERS)-CoV(33). This emphasizes the potential of developing broadly effective vaccines that may cover current and future coronavirus outbreaks. However, in current vaccine development strategies, the S2 subunit is considered as inaccessible, wherein proline mutations are applied to further stabilize the prefusion state. On the contrary, our cryo-ET study here suggests the dynamic nature of the spike protein where parts of the S2 subunit are accessible (Fig. 2c and Fig. 4). As described above, bnAbs may exhibit less potent activity but vaccine-induced bnAbs would overcome this limitation, while the stabilization of the S2 subunit may be necessary. In fact, the development of a multivalent S2-based vaccine was

recently shown to provide a wide effect against beta, delta and omicron variants as well as pangolin coronavirus(32).

Besides the S2 subunit, the currently observed dynamics of the active SARS-CoV-2 virus (Fig. 4) indicates the accessibility of the interface of S1 and S2 subunits. Note that these regions are conserved across SARS-CoV-2 variants. Indeed, the HDX-MS experiment of the recombinant spike protein also shows the increased accessibility of the two subdomains (SD1 and SD2) in the S1 subunit(23). Collectively, accounting for spike dynamics and cryptic epitope formation may facilitate the development of broadly effective vaccines. For instance, a vaccine design based on the spike protomer may better account for spike protein dynamics, exposing cryptic epitopes (Fig. 4 and Fig. S6). To explore monomer dynamics, Molecular Dynamics (MD) simulations of the spike monomer of the Omicron BA.2 variant were performed. Fig. S7 shows that a large range of motions in the S1 subunit can be observed in the absence of the trimeric complex, exposing cryptic pockets located at the interface of the S2 subunit, RBD, and the SD1 subdomain, which may induce a broader spectrum of immune effect. Indeed, monoclonal antibodies (mAbs) targeting cryptic epitopes, such as CR3022, P008-60, and sd1.040, can break up spike trimeric structure(34-36). It is worth mentioning that an early study has reported the feasibility of using a monomeric spike protein of SARS-CoV-1 as a vaccine candidate(37).

Unexpectedly, the active dynamics of the spike protein structure, especially open-trimer conformations, reveal benefits for fusion efficiency. Some portion of open-trimer conformations definitively expose the S2’ cleavage site for TMPRSS2 and cathepsins. In this sense, the spike protein possesses the inherent potential to allow the S1-S2 dissociation, inducing the exposure of the S2’ cleavage site. This process could be further facilitated by the ACE2 binding (Fig. 4). In retrospect, the effect of the D614G mutation would be anticipated to lead to a larger exposure.

The spike protein in active virus is highly dynamic with multiple levels of flexibility including, membrane diffusibility, stalk region knee-like motion(17), RBD Down to Up transition(38) and open-trimer formation(23). In addition, it is highly susceptible to change in temperature, pH and even glycosylation(9, 39). Structural analysis using inactivated viruses or recombinant proteins is essential, however, the effect of mutations, chemical fixations, and trimerization tags shall be considered. Hence, it is crucial to study viral proteins in their native, active state. Cryo-ET at BSL3 facility is expected to be an indispensable method to tackle current and future pandemics.

Materials and Methods

Virus preparation

An ancestral SARS-CoV-2 strain, WK-521 (GISAID: EPI_ISL_408667), was kindly provided by Dr. Shimojima (National Institute of Infectious Diseases, Japan). The viral stock was prepared by the inoculation to Vero E6 cells constantly expressing human TMPRSS2 (Vero E6/TMPRSS2)(40). At 2 days post-infection (dpi), the culturing supernatant was centrifuged at 440 × g for 2 min to remove the cell debris and stored at −80 °C as a virus stock. The titer of the stock was determined by plaque assay as previously described(41). In brief, Vero E6/TMPRSS2 cells were inoculated with serial dilutions of virus stock for 1 h at 37 °C. The cells were overlaid with Dulbecco's Modified Eagle Medium (Nissui) containing 2% FBS and 0.5% Bacto Agar (Becton Dickinson). At 2 dpi, cells were fixed with 3.7% formaldehyde in phosphate-buffered saline (PBS) and stained with 1% crystal violet.

For the preparation of the cryo-ET sample, Vero E6/TMPRSS2 cells in a 6 well plate were inoculated with the virus at a multiplicity of infection (MOI) of 10 and incubated for 1 h at 37 °C. The media was then replaced with 400 µL of fresh Opti-MEM (Thermo Fisher Scientific). At 18 h post-infection, culture supernatant was collected and clarified with 0.45 µm filtration. The sample was kept at 37 °C and used immediately for grid preparation.

Data collection

For cryo-ET, 2 µL of sample was applied on each side of a freshly glow-discharged QUANTIFOIL R 1.2/1.3 Cu 200-mesh grid (Quantifoil Micro Tools). The grid was blotted at once for 15 s from the back side and plunged into liquid ethane using EM GP2 (Leica Microsystems) at 18 °C and 90% humidity chamber setting. The micrograph images were collected on a Krios G4 (Thermo Fisher Scientific) operating at a voltage of 300 kV with an energy filter Selectris (slit width 10 eV) and a direct electron detector Falcon 4. Each micrograph was collected at a nominal magnification of 64,000× (pixel size of 1.88Å) with an exposure time of 0.73 s (dose of 1.5 e/Å2) at a underfocus of 0.2 µm using a Volta phase plate (VPP). Tilt-series data collection was performed with a dose-symmetric scheme tilting by 1° steps from −60° to 60° using Tomography software (Thermo Fisher Scientific), Table S2.

Cryo-Electron Tomography Data Processing.

42 micrographs were processed using the IMOD package(42). Patch tracking was used to align tilt images. Ctfplotter was used to estimate defocus, phase shift, and astigmatism within the context of the contrast transfer function(43). Tomograms were binned 4x and reconstructed with weighted back projection with a voxel size of 7.536 Å. SIRT-like filtered tomograms were generated for visualization and particle picking. Reconstructed tomograms were also imported and filtered in EMAN2(44). Virus particles were manually segmented in EMAN2 and used for isosurface visualization in Chimera-X software(45). The two longest diameters of viruses and the thickness of ice layer were calculated using 3dmod.

291 spike proteins, from 46 virions, were manually picked from the 4-fold binned SIRT tomograms, including pre (247 particles) and postfusion (44 particles) states. The sub-tomogram averaging of the prefusion state were processed in Relion 4.0(26). The reference-free alignment was performed, where the initial map was generated from the binned subtomograms and used

subsequently for other refinements. After obtaining an adequately representative map, the C3 symmetry was invoked. A series of refinements were performed starting from 4x binning to 2x to unbinned. Finally, several cycles of the 3D refinement were performed at a voxel size of 1.884 Å on unbinned subtomograms. After the 3D refinement, the CTF was corrected using ctffind-4.1.14(46) and 2D images alignment was improved in each cycle. The cycles were repeated until no further improvement in resolution was observed. The final average map of the C3 symmetry was estimated to have 14.3 Å resolution at FSC = 0.143 cutoff in RELION4.0. To understand the effect of symmetries, a final cycle of refinement was performed with C1 symmetry, providing a 17.0 Å resolution map. The models of the spike protein, PDB 6ZGE and 7M0J, were rigid fitted in the C3 map using ChimeraX(45). PyMOL software was used for visualizing the structures (47).

References and Notes

1. B. Hu, H. Guo, P. Zhou, Z. L. Shi, Characteristics of SARS-CoV-2 and COVID-19. *Nat Rev Microbiol* **19**, 141-154 (2021).
2. Y. Cao *et al.*, Omicron escapes the majority of existing SARS-CoV-2 neutralizing antibodies. *Nature* **602**, 657-663 (2022).
3. T. Tamura *et al.*, Virological characteristics of the SARS-CoV-2 XBB variant derived from recombination of two Omicron subvariants. *Nat Commun* **14**, 2800 (2023).
4. J. W. Saville, A. M. Berezuk, S. S. Srivastava, S. Subramaniam, Three-Dimensional Visualization of Viral Structure, Entry, and Replication Underlying the Spread of SARS-CoV-2. *Chem Rev* **122**, 14066-14084 (2022).
5. Q. Wang *et al.*, Structural and Functional Basis of SARS-CoV-2 Entry by Using Human ACE2. *Cell* **181**, 894-904 e899 (2020).
6. Y. Cai *et al.*, Distinct conformational states of SARS-CoV-2 spike protein. *Science* **369**, 1586-1592 (2020).
7. C. Xu, W. Han, Y. Cong, Cryo-EM and cryo-ET of the spike, virion, and antibody neutralization of SARS-CoV-2 and VOCs. *Curr Opin Struct Biol* **82**, 102664 (2023).
8. D. Wrapp *et al.*, Cryo-EM structure of the 2019-nCoV spike in the prefusion conformation. *Science* **367**, 1260-1263 (2020).
9. T. Zhou *et al.*, Cryo-EM Structures of SARS-CoV-2 Spike without and with ACE2 Reveal a pH-Dependent Switch to Mediate Endosomal Positioning of Receptor-Binding Domains. *Cell Host Microbe* **28**, 867-879 e865 (2020).
10. A. G. Wrobel *et al.*, SARS-CoV-2 and bat RaTG13 spike glycoprotein structures inform on virus evolution and furin-cleavage effects. *Nat Struct Mol Biol* **27**, 763-767 (2020).
11. X. Fan, D. Cao, L. Kong, X. Zhang, Cryo-EM analysis of the post-fusion structure of the SARS-CoV spike glycoprotein. *Nat Commun* **11**, 3618 (2020).
12. A. Saito *et al.*, Virological characteristics of the SARS-CoV-2 Omicron BA.2.75 variant. *Cell Host Microbe* **30**, 1540-1555 e1515 (2022).
13. V. Mangala Prasad *et al.*, Cryo-ET of Env on intact HIV virions reveals structural variation and positioning on the Gag lattice. *Cell* **185**, 641-653 e617 (2022).
14. L. J. Calder, T. Calcraft, S. Hussain, R. Harvey, P. B. Rosenthal, Electron cryotomography of SARS-CoV-2 virions reveals cylinder-shaped particles with a double layer RNP assembly. *Commun Biol* **5**, 1210 (2022).
15. Y. Song *et al.*, In situ architecture and membrane fusion of SARS-CoV-2 Delta variant. *Proc Natl Acad Sci U S A* **120**, e2213332120 (2023).
16. H. Yao *et al.*, Molecular Architecture of the SARS-CoV-2 Virus. *Cell* **183**, 730-738 e713 (2020).
17. B. Turonova *et al.*, In situ structural analysis of SARS-CoV-2 spike reveals flexibility mediated by three hinges. *Science* **370**, 203-208 (2020).
18. L. Mendonca *et al.*, Correlative multi-scale cryo-imaging unveils SARS-CoV-2 assembly and egress. *Nat Commun* **12**, 4629 (2021).
19. L. Zimmermann, P. Chlanda, Cryo-electron tomography of viral infection - from applications to biosafety. *Curr Opin Virol* **61**, 101338 (2023).
20. C. L. Hsieh *et al.*, Structure-based design of prefusion-stabilized SARS-CoV-2 spikes. *Science* **369**, 1501-1505 (2020).
21. J. Juraszek *et al.*, Stabilizing the closed SARS-CoV-2 spike trimer. *Nat Commun* **12**, 244 (2021).

22. M. Claireaux *et al.*, A public antibody class recognizes an S2 epitope exposed on open conformations of SARS-CoV-2 spike. *Nat Commun* **13**, 4539 (2022).
23. S. M. Costello *et al.*, The SARS-CoV-2 spike reversibly samples an open-trimer conformation exposing novel epitopes. *Nat Struct Mol Biol* **29**, 229-238 (2022).
24. T. Ichikawa *et al.*, Chemical fixation creates nanoscale clusters on the cell surface by aggregating membrane proteins. *Commun Biol* **5**, 487 (2022).
25. R. P. Silva *et al.*, Identification of a conserved S2 epitope present on spike proteins from all highly pathogenic coronaviruses. *Elife* **12**, (2023).
26. J. Zivanov *et al.*, A Bayesian approach to single-particle electron cryo-tomography in RELION-4.0. *Elife* **11**, (2022).
27. S. Bangaru *et al.*, Structural analysis of full-length SARS-CoV-2 spike protein from an advanced vaccine candidate. *Science* **370**, 1089-1094 (2020).
28. S. M. Gobeil *et al.*, Effect of natural mutations of SARS-CoV-2 on spike structure, conformation, and antigenicity. *Science* **373**, (2021).
29. R. Henderson *et al.*, Controlling the SARS-CoV-2 spike glycoprotein conformation. *Nat Struct Mol Biol* **27**, 925-933 (2020).
30. H. M. Dokainish, Y. Sugita, Structural effects of spike protein D614G mutation in SARS-CoV-2. *Biophys J* **122**, 2910-2920 (2023).
31. D. Zhou, J. Ren, E. E. Fry, D. I. Stuart, Broadly neutralizing antibodies against COVID-19. *Curr Opin Virol* **61**, 101332 (2023).
32. P. J. Halfmann *et al.*, Multivalent S2-based vaccines provide broad protection against SARS-CoV-2 variants of concern and pangolin coronaviruses. *EBioMedicine* **86**, 104341 (2022).
33. T. A. Olukitibi *et al.*, Significance of Conserved Regions in Coronavirus Spike Protein for Developing a Novel Vaccine against SARS-CoV-2 Infection. *Vaccines (Basel)* **11**, (2023).
34. J. Huo *et al.*, Neutralization of SARS-CoV-2 by Destruction of the Prefusion Spike. *Cell Host Microbe* **28**, 445-454 e446 (2020).
35. J. Seow *et al.*, A neutralizing epitope on the SD1 domain of SARS-CoV-2 spike targeted following infection and vaccination. *Cell Rep* **40**, 111276 (2022).
36. F. Bianchini *et al.*, Human neutralizing antibodies to cold linear epitopes and subdomain 1 of the SARS-CoV-2 spike glycoprotein. *Sci Immunol* **8**, eade0958 (2023).
37. J. Li, L. Ulitzky, E. Silberstein, D. R. Taylor, R. Viscidi, Immunogenicity and protection efficacy of monomeric and trimeric recombinant SARS coronavirus spike protein subunit vaccine candidates. *Viral Immunol* **26**, 126-132 (2013).
38. H. M. Dokainish *et al.*, The inherent flexibility of receptor binding domains in SARS-CoV-2 spike protein. *Elife* **11**, (2022).
39. A. S. Olia *et al.*, SARS-CoV-2 S2P spike ages through distinct states with altered immunogenicity. *J Biol Chem* **297**, 101127 (2021).
40. M. Sasaki *et al.*, SARS-CoV-2 Bearing a Mutation at the S1/S2 Cleavage Site Exhibits Attenuated Virulence and Confers Protective Immunity. *mBio* **12**, e0141521 (2021).
41. M. Sasaki *et al.*, S-217622, a SARS-CoV-2 main protease inhibitor, decreases viral load and ameliorates COVID-19 severity in hamsters. *Sci Transl Med* **15**, eabq4064 (2023).
42. J. R. Kremer, D. N. Mastronarde, J. R. McIntosh, Computer visualization of three-dimensional image data using IMOD. *J Struct Biol* **116**, 71-76 (1996).
43. Q. Xiong, M. K. Morphew, C. L. Schwartz, A. H. Hoenger, D. N. Mastronarde, CTF determination and correction for low dose tomographic tilt series. *J Struct Biol* **168**, 378-387 (2009).

44. G. Tang *et al.*, EMAN2: an extensible image processing suite for electron microscopy. *J Struct Biol* **157**, 38-46 (2007).
45. E. F. Pettersen *et al.*, UCSF ChimeraX: Structure visualization for researchers, educators, and developers. *Protein Sci* **30**, 70-82 (2021).
46. A. Rohou, N. Grigorieff, CTFFIND4: Fast and accurate defocus estimation from electron micrographs. *J Struct Biol* **192**, 216-221 (2015).
47. Schrodinger, LLC.

Acknowledgments: We thank Hiroshi Kida, Tatsuya Zenko, Atsushi Furukawa, Takashi Tadokoro, Robert Parsons, Peijun Zhang, Fabian Eisenstein, Radostin Danev, Makoto Takeda for their support and discussions. We also thank members of Facilities Division of Hokkaido University and Thermofisher Scientific (Yoshihiro Tomatsu, Kazuhiro Aoyama, Yu Yong) for their technical assistance.

Funding:
Japan Agency for Medical Research and Development (AMED) [JP17am0101093 (K.M.)]
Japan Agency for Medical Research and Development (AMED) [JP20ae0101047 (K.M.)]
Japan Agency for Medical Research and Development (AMED) [JP21fk0108463 (K.M.)]
Japan Agency for Medical Research and Development (AMED) [JP22ama121037 (K.M.)]
Japan Agency for Medical Research and Development (AMED) [JP223fa627005 (K.M, K.T, M.S, Y.O, and H.S.)]
Japan Agency for Medical Research and Development (AMED) [JP23ama121001 (T.S.)]
Hokkaido University Biosurface project (K.M.)
Japan Science and Technology Agency (JST) CREST grant number JPMJCR20H8 (H.F)
JSPS Strategic Young Researcher Overseas Visits Program for Accelerating Brain Circulation (K.M.)
The Scientific Research on Innovative Areas and International Group from the MEXT/JSPS KAKENHI [JP20H05873 (K.M)]
Ministry of Health, Labour and Welfare (MHLW) [23HA2010 (H.S.)]
Takeda Science Foundation (K.M.)
Computational resources of the supercomputer Fugaku provided by the RIKEN Center for Computational Science [hp230052 (H.M.D.)]
Computational resources of the supercomputer Fugaku provided by the RIKEN Center for Computational Science [hp220087 (H.M.D)]

Author contributions:
Designed the study: H.F., H.M.D., and K.M
Set up BSL3 Cryo-EM facility: H.F., S.K., Y.S., H.S. and K.M.
Assisted to set up and consult about BSL3 Cryo-EM facility: J.T.H. and D.I.S.
Prepared virus solution: H.F., K.T, M.S., Y.O., and H.S
Performed cryo-ET data collection: H.F., S.K., K.T., Y.A., and H.S.
Performed cryo-ET analysis: H.M.D.
Advised Cryo-ET analysis S.K., J.T.H., and K.M.
Designed and prepared unique device of sample transfer for Cryo-ET: A.S. T.S., and K.M.
Wrote the manuscript: H.M.D., H.F., and K.M.

Competing interests: Authors declare that they have no competing interests.

Data and materials availability: All other data are available from the corresponding author upon request.

Supplementary Materials

Materials and Methods

Figs. S1 to S7

Tables S1 to S2

References (*1*–*9*)

Movies S1 to S4

Figure 1. Pleomorphology of active virus particles. a) Central sections (7.5 nm thick) through the cryo-ET tomograms of the ancestral virions. b) Violin plot representation of the two longest diameters (L1 and L2) in 46 virus particles. c) Tomograms slices of three virions with very large diameters (Left: L1:139, L2:102; Middle: L1:125, L2:119; Right: L1:150, L2:125). d) Central slices of virions on carbon film.

Figure 2. Distribution and atypical conformations of the spike protein. a) The 2D central slice of virus particle showing the formation of higher order structures including dimer of trimers and trimer of trimers. Isosurface is also shown in mesh representation, wherein PDB 6ZGE[10] is fitted and shown in surface representation. b) Tomograms slices (7.5 nm thick) of four virions with clusters of postfusion spike structures. Postfusion conformations are highlighted with white arrowheads. c) The isosurface representation of several spike proteins on the virus surface, wherein the closed/packed and open trimers of prefusion states can be identified as shown by dashed lines. d) The magnified view of 2D central slice tomograms of the typical spike protein densities including Down, 1Up, 2Up and 3Up conformations, as well as atypical spike protein densities observed in active viruses. The detached S1 subunits are highlighted by dashed lines. e) Proposed schematic representation of the spike opening mechanism at prefusion states, in which one protomer S1 subunit undergoes a large conformational change. f) Magnified views of tomogram slices of different forms of atypical spike trimer/monomers. See Fig. S3b for zoomed out views.

Figure 3. The spike protein averaged map obtained by SPT analysis. a) The sub-tomogram averaged map with the superimposition of cryo-EM structures of the spike trimer (PDB 7M0J; Top)) and (PDB 6ZGE; Bottom). Purple, green and pink colors were used to represent spike protomers. The zoomed-in view of the trimeric S2 interface from 7M0J (pink and green ribbons) and 6ZGE (blue ribbon), fitted into the spike protein average map (Top center), indicating the S2 variation in fitted middle helices. The zoomed-in view of the terminal part of spike protein averaged map (Bottom center) with fitted PDB structures, 7M0J (pink, green and purple ribbons) and 6ZGE (blue ribbon). Arrows in central panels indicate structural shifts from 6ZGE to 7M0J. b) Top views of the sub-tomogram averaged maps of the C3 symmetry (top) and the C1 symmetry (bottom) fitted with prefusion-state spike protein (PDB 7M0J).

Figure 4. Proposed model of spike structural changes for the membrane fusion. (top right panel) Schematic representation of the spike structure with the domain organization. The color of each protomer corresponds to Fig. 2e. (top left to center) New cryptic sites of the S2 subunit exposed in open-trimer conformations of the spike protein, potential targets for vaccine and antibodies/drugs. (bottom) Schematic presentation of the proposed fusion mechanism. Fixed or recombinant spikes protein take a closed or Up RBD structure (gray box). On the active virus, spike proteins exist as a loosely packed trimer, with a partially opened S1 subunit. When the ACE2 binding promotes the S2 subdomain exposure, the S2 subunit irreversibly refolds to the postfusion state to fuse the viral envelope with the host cell membrane.

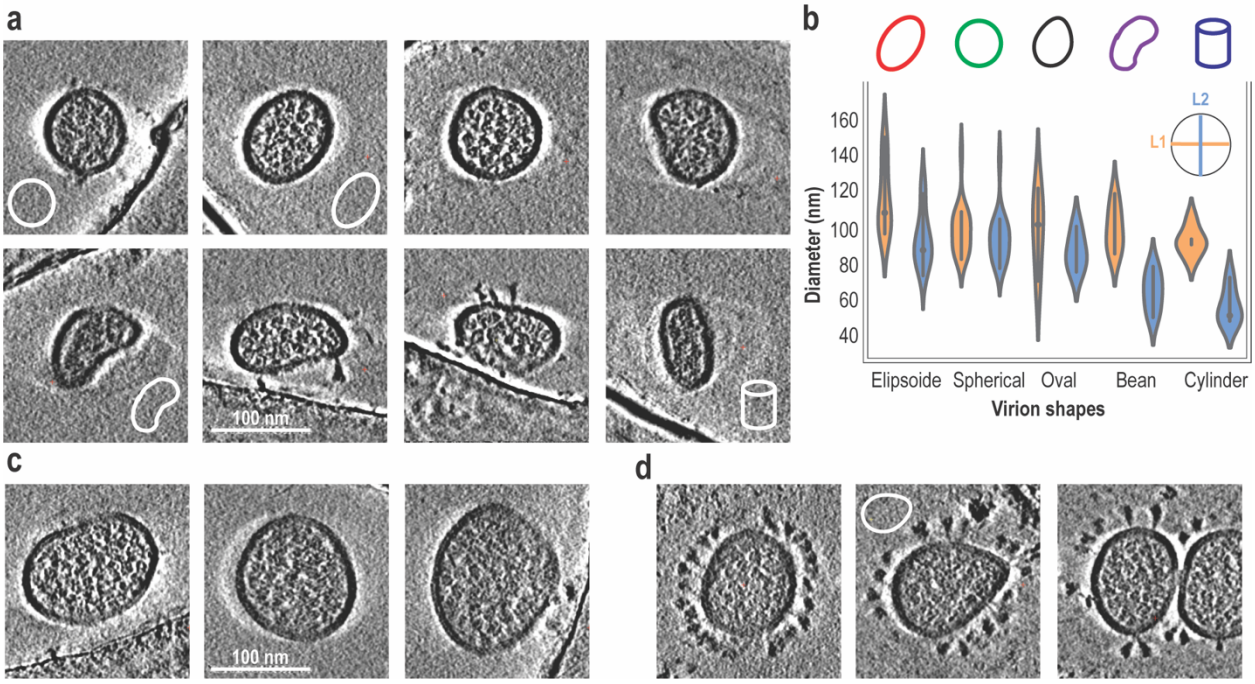

Figure 1. Pleomorphology of active virus particles. a) Central sections (7.5 nm thick) through the cryo-ET tomograms of the ancestral virions. b) Violin plot representation of the two longest diameters (L1 and L2) in 46 virus particles. c) Tomograms slices of three virions with very large diameters (Left: L1:139, L2:102; Middle: L1:125, L2:119; Right: L1:150, L2:125). d) Central slices of virions on carbon film.

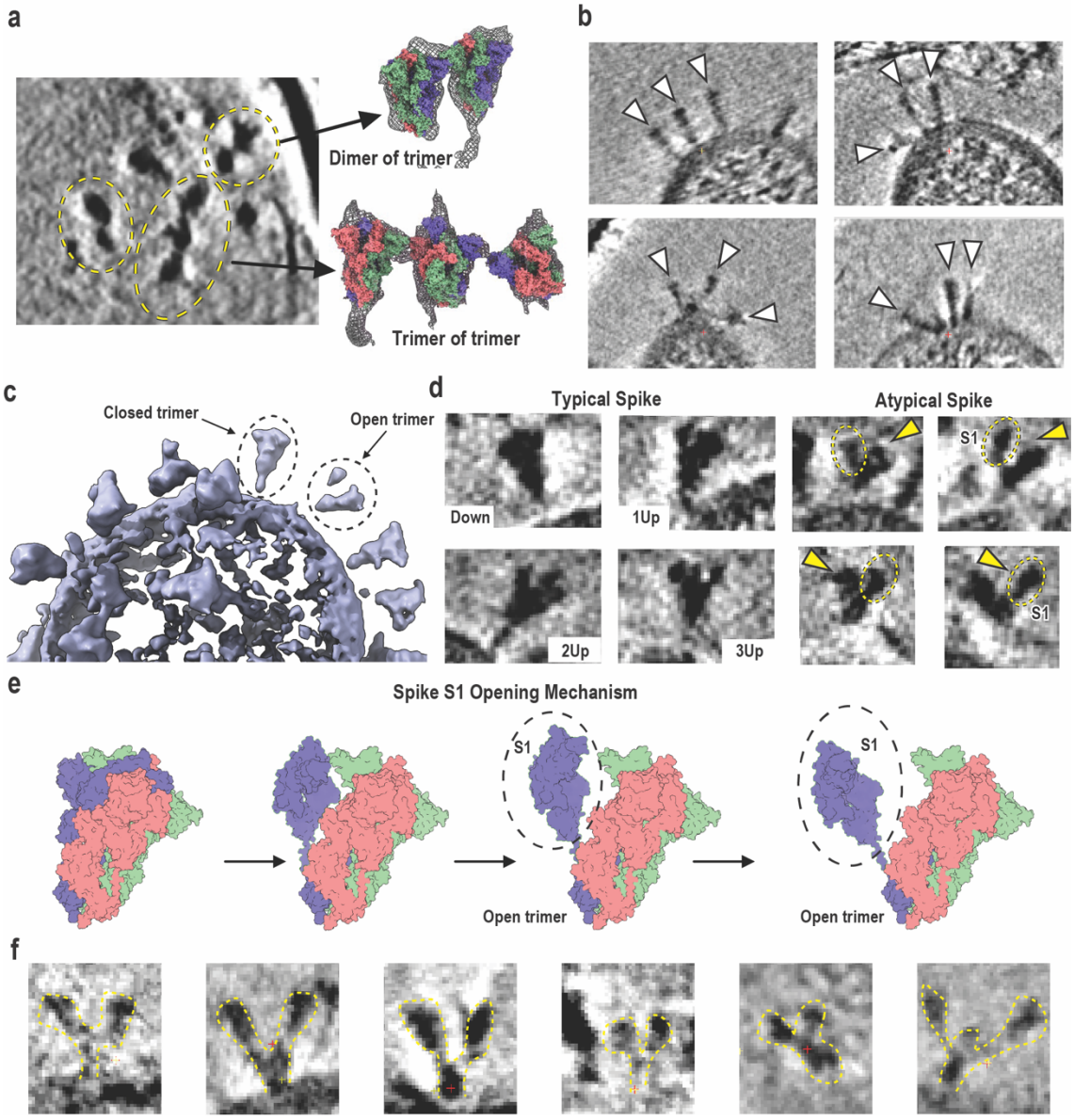

Figure 2. Distribution and atypical conformations of the spike protein. a) The 2D central slice of virus particle showing the formation of higher order structures including dimer of trimers and trimer of trimers. Isosurface is also shown in mesh representation, wherein PDB 6ZGE[10] is fitted and shown in surface representation. b) Tomograms slices (7.5 nm thick) of four virions with clusters of postfusion spike structures. Postfusion conformations are highlighted with white arrowheads. c) The isosurface representation of several spike proteins on the virus surface, wherein the closed/packed and open trimers of prefusion states can be identified as shown by dashed lines. d) The

magnified view of 2D central slice tomograms of the typical spike protein densities including Down, 1Up, 2Up and 3Up conformations, as well as atypical spike protein densities observed in active viruses. The detached S1 subunits are highlighted by dashed lines. e) Proposed schematic representation of the spike opening mechanism at prefusion states, in which one protomer S1 subunit undergoes a large conformational change. f) Magnified views of tomogram slices of different forms of atypical spike trimer/monomers. See Fig. S3b for zoomed out views.

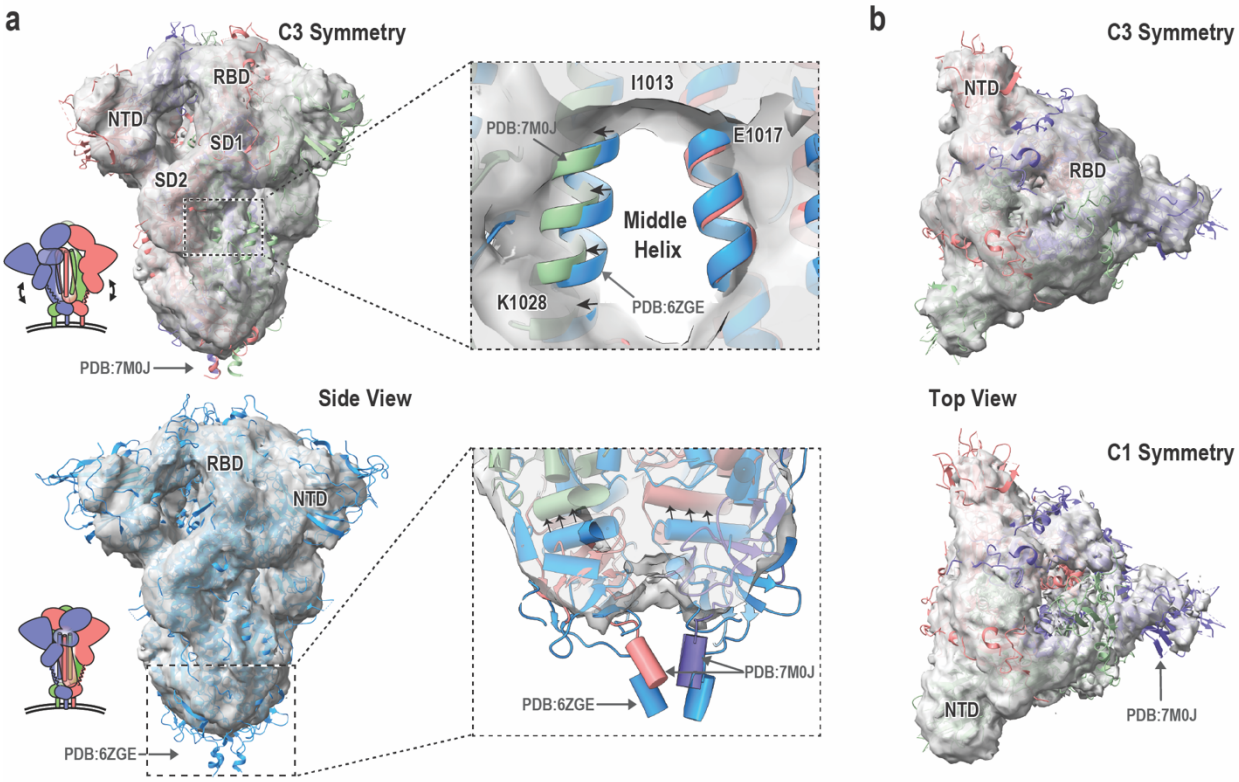

Figure 3. The spike protein averaged map obtained by SPT analysis. a) The sub-tomogram averaged map with the superimposition of cryo-EM structures of the spike trimer (PDB 7M0J; Top)) and (PDB 6ZGE; Bottom). Purple, green and pink colors were used to represent spike protomers. The zoomed-in view of the trimeric S2 interface from 7M0J (pink and green ribbons) and 6ZGE (blue ribbon), fitted into the spike protein average map (Top center), indicating the S2 variation in fitted middle helices. The zoomed-in view of the terminal part of spike protein averaged map (Bottom center) with fitted PDB structures, 7M0J (pink, green and purple ribbons) and 6ZGE (blue ribbon). Arrows in central panels indicate structural shifts from 6ZGE to 7M0J. b) Top views of the sub-tomogram averaged maps of the C3 symmetry (top) and the C1 symmetry (bottom) fitted with prefusion-state spike protein (PDB 7M0J).

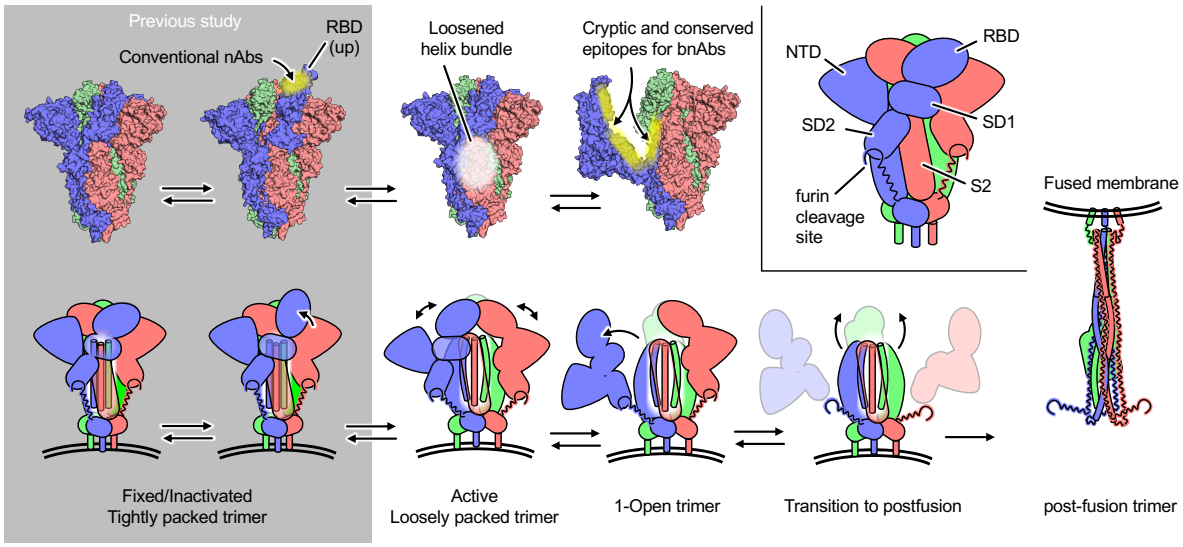

Figure 4. Proposed model of spike structural changes for the membrane fusion. (top right panel) Schematic representation of the spike structure with the domain organization. The color of each protomer corresponds to Fig. 2e. (top left to center) New cryptic sites of the S2 subunit exposed in open-trimer conformations of the spike protein, potential targets for vaccine and antibodies/drugs. (bottom) Schematic presentation of the proposed fusion mechanism. Fixed or recombinant spikes protein take a closed or Up RBD structure (gray box). On the active virus, spike proteins exist as a loosely packed trimer, with a partially opened S1 subunit. When the ACE2 binding promotes the S2 subdomain exposure, the S2 subunit irreversibly refolds to the postfusion state to fuse the viral envelope with the host cell membrane.